

Induced-charge electrophoresis of a tilted metal nanowire near an insulating wallJose Eladio Flores-Mena ¹, Pablo García-Sánchez ², and Antonio Ramos ²¹*Facultad de Ciencias de la Electrónica, Benemérita Universidad Autónoma de Puebla, Av. San Claudio y 18 Sur, San Manuel, CU. FCE2, 72570 Puebla, Mexico*²*Departamento de Electrónica y Electromagnetismo, Facultad de Física, Universidad de Sevilla, Avda. Reina Mercedes s/n, 41012 Sevilla, Spain*

(Received 29 November 2023; accepted 11 April 2024; published 30 April 2024)

Electric fields are commonly used to control the orientation and motion of microscopic metal particles in aqueous suspensions. For example, metallodielectric Janus spheres are propelled by the induced-charge electro-osmotic flow occurring on their metallic side, the most common case in electrokinetics of exploiting symmetry breaking of surface properties for achieving net particle motion. In this work, we demonstrate that a homogeneous metal rod can translate parallel to a dielectric wall as a result of the hydrodynamic wall-particle interaction arising from the induced-charge electro-osmosis on the rod surface. The applied electric field could be either dc or low-frequency ac. The only requirement for a nonvanishing particle velocity is that the axis of the rod be inclined with respect to the wall, i.e., it cannot be neither parallel nor perpendicular. We show numerical results of the rod velocity as a function of rod orientation and distance to the wall. The maximum particle velocity is found for an orientation of between $\sim 30^\circ$ and $\sim 50^\circ$, depending on the position and aspect ratio of the cylinder. Particle velocities of up to tens of $\mu\text{m/s}$ are predicted for typical conditions in electrokinetic experiments.

DOI: [10.1103/PhysRevE.109.045109](https://doi.org/10.1103/PhysRevE.109.045109)**I. INTRODUCTION**

Electric fields are commonly used to induce the motion of small particles immersed in water or other liquids. For example, electrophoresis describes the motion of a particle in an electrolyte due to the interaction of an electric field with electrical charges in the electrical double layer (EDL) at the particle-electrolyte interface [1,2]. Electrophoresis is extensively used for the analysis and separation of colloids [3], macromolecules such as DNA and proteins [4], and, in general, any particle that carries a net surface charge when suspended in an electrolyte. Particles that remain uncharged when dispersed in water are not prone to electrophoretic manipulation, but other electrokinetic phenomena can be harnessed. For example, metallodielectric Janus spheres are microscopic spheres with half of their surface covered by a metal while the other half is of a dielectric material. When these microspheres are dispersed in electrolytes, they are translated in a direction perpendicular to the applied electric field [5]. This motion has its origin in the electro-osmotic induced charge flow (ICEO) [6,7] that occurs on the metallic side of the Janus microspheres, a kind of electrokinetic flow that does not appear on the dielectric side of the particle. The net motion of the Janus sphere is named ICEP (induced-charge electrophoresis) and has its origin in the action of the electric field in the EDL due to induced charges on a metal surface rather than on intrinsic charges, as in “classical” electrophoresis. ICEP of Janus spheres is the most common example of net motion that appears when symmetry is broken in ICEO systems [8–11]. Another example of particle motion due to symmetry breaking of the electrokinetic flow was recently reported by Katzmeier *et al.* [12], where dimers of microparticles of different sizes are translated due to asymmetric concentration polarization electro-osmosis [13,14].

In most experimental situations, particles are translated adjacent to the bottom substrate of a microfluidic chamber as a result of buoyancy mismatch. While the presence of a wall is commonly seen as a nuisance, the wall-particle interaction gives rise to a net motion of the particle, opening opportunities for self-propulsion mechanisms. For example, it is shown in [15] that a Janus sphere sitting on an electrode moves in a direction opposite to the ICEP motion if the frequency of the ac field is high (> 10 kHz). This motion was termed self-dielectrophoresis (sDEP) and it has been shown that this dielectrophoretic-type force arises when the EDL induced at the electrode-electrolyte interface is considered in the study of the particle-electrode interaction [16] (i.e., a particle sitting on a nonpolarizable electrode does not undergo sDEP motion). The motion of Janus particles near an insulating wall was first theoretically described by Kilic and Bazant [17]. Another example of electrokinetic particle motion due to the interaction with a wall was reported in [18], where dielectric colloidal dimers with broken symmetry sit on an electrode and move horizontally. The difference between the two colloidal particles can be in geometry, composition, or interfacial charges, and it gives rise to unbalanced electrohydrodynamic flows, which induce the motion of the dimer.

In this work we study the interaction of ICEO flows around a metal nanowire and a nearby insulating flat wall. We show that the nanowire is translated when it is inclined with respect to the wall, in contrast to the case of a nanowire in the liquid bulk, which aligns with the direction of the electric field but does not translate [19,20]. The experimental results in these works show that the orientation time is very short (less than 1 s). Thus we expect negligible displacement of the nanowire unless its orientation is fixed by an external torque (see Appendix B). In the present work, we assume that the

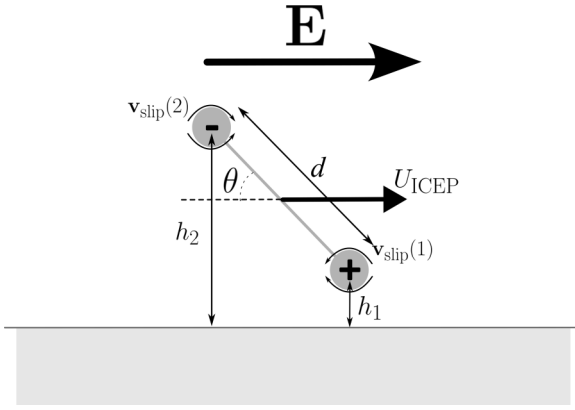


FIG. 1. Model particle consisting of two metal spheres connected by a thin metal wire. The electro-osmotic velocities induced on the spheres give rise to an interaction with the wall that leads to a net particle velocity U_{ICEP} . The sphere closest to the wall leads the motion. Note that this is the direction of the motion regardless of the sign of the applied electric field, as expected for the ICEP.

orientation of the cylinder axis does not change during its translation. For example, Haque *et al.* [21] used magnetic fields to fix the orientation of magnetic colloidal chains, similar to cylindrical rods, to induce electrokinetic particle motion near electrodes.

The electrokinetic manipulation of metal and semiconductor nanowires in suspension has been extensively studied by our group [20,22–24] and others [25–32]. As happens for conducting particles [33–36], their electrokinetic behavior is determined by the polarization of the EDL at the particle-electrolyte interface, which is induced by the applied electric field. This polarization mechanism gives rise to the ICEO flows around the nanowire and, as mentioned above, in this work we show that the interaction of these flows with a wall can result in translation of the nanowire.

In the next section of this paper, we show a heuristic model that predicts the net motion of an elongated metal particle near a wall. Then, the theoretical analysis for the ICEP of a metal cylinder is presented. We show numerical results for the velocity of the cylinder at a distance of a wall and as a function of its orientation. The maximum velocity of the nanowire is found for an orientation between $\sim 30^\circ$ and $\sim 55^\circ$, depending on the position and aspect ratio of the cylinder.

II. HEURISTIC MODEL FOR THE ICEP MOTION OF AN ELONGATED PARTICLE NEAR A WALL

The ICEP motion of an elongated metal particle can be qualitatively understood if we consider a model particle consisting of two metal spheres of radius R connected by a thin and long conducting wire with length $d \gg R$ (see Fig. 1)—this approximation allows us to neglect any hydrodynamic interaction between spheres. The ICEP motion of composite particles formed by two spheres with different radii and away from the wall was considered by Squires and Bazant [8]. We assume that the spheres are initially uncharged and, upon application of an electric field, charges of opposite signs are induced on the two spheres. These charges are screened by ions in the electrolyte, building electrical double layers (EDL)

around the metal particles. In this situation, the voltage drop across the EDL can be written as $\zeta_1 = dE \cos(\theta)/2$ for sphere 1 and $\zeta_2 = -dE \cos(\theta)/2$ for sphere 2. This voltage drop is known as zeta potential (ζ) and is of crucial importance in electrokinetics since the electrophoretic velocity is given by the Helmholtz-Smoluchowski equation [1]:

$$v_{\text{HS}} = -(\varepsilon \zeta E)/\eta, \quad (1)$$

where ε and η are, respectively, the electrical permittivity and the viscosity of the electrolyte. Expression (1) is valid when the thickness of the EDL is much smaller than the size of the particle.

We aim to calculate the ICEP velocity (U_{ICEP}) of the composite particle in Fig. 1 that arises from the electro-osmosis on the surface of the two spheres. We assume that the orientation of the particles is kept fixed by an external torque. The ICEP motion is a force-free motion with a fluid velocity field that can be decomposed into the following two problems: (i) the velocity field due to a stationary particle ($U = 0$) with slip velocities on the spheres $v_{\text{slip}(i)}$, $i = \{1, 2\}$, and (ii) the velocity field due to a particle moving with velocity $U = U_{\text{ICEP}}$ and zero slip velocity on the spheres. To keep the particle stationary in problem (i), there must be an applied external force corresponding to the sum of the forces required to keep the two spheres stationary. According to Keh and Anderson [37], including a first-order correction to the electrophoretic velocity of a sphere moving parallel to a wall results in the following expression:

$$\mathbf{U}_{\text{elpho}} = (1 - \lambda^3/16) \frac{\varepsilon \zeta}{\eta} \mathbf{E}, \quad (2)$$

where $\lambda = R/h$, with h the distance of the center of the sphere to the wall. Thus the electrophoretic velocities of the two spheres of Fig. 1 can be written as $\mathbf{U}_{\text{elpho}(i)} = \frac{\varepsilon \zeta_i \mathbf{E}}{\eta} (1 - \lambda_i^3/16)$; $i = \{1, 2\}$. Also, the viscous friction coefficient γ for a sphere moving parallel to a wall in the leading order in λ is [38]

$$\gamma = 6\pi\eta R/[1 - (9/16)\lambda]. \quad (3)$$

Here, we have neglected the hydrodynamic interaction between spheres. This holds as long as $h_i \ll d$.

The external force to keep the composite particle stationary is $\mathbf{F}_{\text{external}} = -\sum_i \gamma_i \mathbf{U}_{\text{elpho}(i)}$. Likewise, the viscous force in problem (ii) is $\mathbf{F}_{\text{ICEP}} = -(\gamma_1 + \gamma_2) \mathbf{U}_{\text{ICEP}}$. Since the problem is force free ($\mathbf{F}_{\text{ICEP}} + \mathbf{F}_{\text{external}} = 0$), the leading term of the ICEP velocity is

$$\begin{aligned} U_{\text{ICEP}} &\approx \frac{\gamma_1 - \gamma_2}{\gamma_1 + \gamma_2} [\varepsilon d \cos(\theta)/2\eta] E^2 \\ &\approx \frac{9(\lambda_1 - \lambda_2)}{32} [\varepsilon d \cos(\theta)/2\eta] E^2. \end{aligned} \quad (4)$$

If sphere 1 is closer to the wall than sphere 2, $\lambda_1 > \lambda_2$, and the model predicts the motion of the composite particle with sphere 1 leading. Note that this is the direction of the motion regardless of the sign of the applied electric field, as expected for the ICEP motion. This result can be explained by considering that the force exerted by the wire is the same on each particle. The perturbation in their velocities is not symmetric since the correction to the drag coefficient due to the presence of the wall scales as (R/h) . Thus the sphere closest

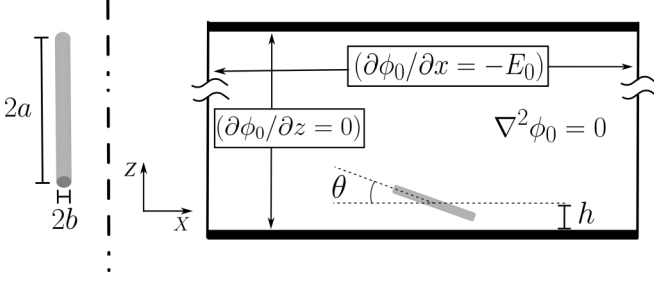


FIG. 2. Schematics of the physical problem. A metallic cylinder with length $2a$ and diameter $2b$ lies at a distance h over a flat wall. The top wall is very far from the cylinder. There is a dc or low-frequency applied electric field in the horizontal direction.

to the wall has a higher drag coefficient and, consequently, it is less affected by the presence of the other particle.

Additionally, we can use this model to calculate the external torque required to fix the particle orientation. Since $\lambda_i \ll 1$, the magnitude of the external torque is $N = (3/2)\pi R d^2 \varepsilon E^2 \sin(2\theta)$.

III. THEORETICAL ANALYSIS FOR A METALLIC CYLINDER

Consider a metallic cylinder immersed in an aqueous electrolyte. The center of the cylinder is at a distance h over the bottom wall of the electrolyte container and its axis forms an angle θ with respect to the horizontal; see Fig. 2. The length and diameter of the cylinder are, respectively, $2a$ and $2b$. Thus the aspect ratio of the cylinder is $\beta = b/a$.

The metallic cylinder is subjected to a homogeneous ac electric field with amplitude $E_0 \mathbf{u}_x$ and angular frequency ω , $\mathbf{E} = E_0 \cos(\omega t) \mathbf{u}_x$. We assume that the metal-electrolyte interface is perfectly polarizable, i.e., it blocks the passage of ions or electrons. In this situation, the electrical current in the electrolyte induces an electrical double layer (EDL) on the surface of the particle [39]. The characteristic thickness of the EDL is given by the Debye length [1], which ranges around tens of nanometers for typical values of the electrolyte conductivities used in experiments. Therefore, it is common to make the approximation of thin EDL for metal rods with diameters of hundreds of nanometers [40]. In this approximation, the system can be described as an electroneutral electrolyte in contact with the surface of the particle that behaves as an ideal capacitor [41,42]—with a value for surface capacitance determined by the EDL capacitance. Then, the electric field in the liquid can be derived from an electric potential $[\mathbf{E}(\mathbf{r}, t) = -\nabla\phi(\mathbf{r}, t)]$, with $\phi(\mathbf{r}, t) = \phi_0(\mathbf{r}) \cos(\omega t)$ and $\phi_0(\mathbf{r})$ the solution of the Laplace equation. For simplicity, we assume that the frequency of the applied electric field is low and that the EDL is fully charged. This means that the currents surround the particle and, therefore, we impose $\mathbf{n} \cdot \mathbf{J} = 0$ on the surface of the particle, where \mathbf{J} is the current density and \mathbf{n} is a normal vector to the surface. This transforms into the following boundary condition for the electric potential on the surface of the particle: $\mathbf{n} \cdot \nabla\phi_0 = 0$. The same boundary condition applies to the top and bottom walls of the electrolyte container, which are insulating (see Fig. 2). We consider that the top wall is very far from the bottom, ideally infinitely far.

A. Induced-charged electro-osmosis on a metal particle

Following the description above, the applied electric field builds an EDL on the surface of the metal particle. The electric field, which is tangent to the particle surface, acts on the charge of the EDL and gives rise to an electro-osmotic slip velocity. This flow is known as induced-charge electro-osmosis (ICEO) [6], and the slip velocity is given by the following expression:

$$\mathbf{v}_s = -\frac{\varepsilon}{4\eta} \nabla_t |\phi_0 - V|^2, \quad (5)$$

where η is the viscosity of the electrolyte, ∇_t is the component of the gradient operator tangential to the particle surface, and V is the amplitude of the electric potential of the floating metal particle. For simplicity, we choose the particle potential as the origin of the electric potential. Thus $V = 0$ and the ICEO slip velocity is written as

$$\mathbf{v}_s = -\frac{\varepsilon}{4\eta} \nabla_t |\phi_0|^2. \quad (6)$$

B. Particle velocity and reciprocity theorem

Since we have fixed the orientation of the cylinder, the velocity of the fluid on its surface can be written as $\mathbf{v} = \mathbf{v}_s + \mathbf{U}$, where \mathbf{U} is the velocity of the center of mass of the particle. In this work, we are interested in calculating \mathbf{U} , which arises from the hydrodynamic interaction of the ICEO flows with the nearby walls. Since we fixed the particle height, the particle motion is restricted to the horizontal direction and its velocity can be written as $\mathbf{U}_{\text{ICEP}} = U_{\text{ICEP}} \mathbf{u}_x$, where ICEP indicates *induced charge electrophoresis*. Knowing the slip velocity on the particle, U_{ICEP} can be calculated if we make use of the Lorentz reciprocity theorem [43–46]:

$$U_{\text{ICEP}} = -\frac{\int_S (\mathbf{n} \cdot \mathbb{T} \cdot \mathbf{v}_s) dS}{\int_S (\mathbf{n} \cdot \mathbb{T} \cdot \mathbf{u}_x) dS}, \quad (7)$$

where \mathbb{T} is the hydrodynamic stress tensor in the liquid due to the cylinder moving with a certain speed in the horizontal direction, S is a closed surface bounding the fluid, and \mathbf{n} is a unit vector normal to S . Since the velocity of the liquid is zero at all boundaries except the surface of the particle, S in Eq. (7) reduces to the surface of the particle. The denominator in Eq. (7) corresponds to the horizontal component of the viscous force acting on the cylinder when moving with velocity $\mathbf{U} = U \mathbf{u}_x$.

Equation (7) provides a way to calculate the velocity of the ICEP of the particles without solving the fluid velocity field (Stokes problem) induced by the slip velocity. Instead, we only need to know the hydrodynamic stress tensor associated with the velocity field induced by a particle moving within the fluid. We chose this method because of its elegance and for maintaining the formulation of previous works with arbitrary frequency ac fields, where we used the reciprocity theorem to reduce the workload of numerical calculations [23,47,48].

IV. NUMERICAL RESULTS

For evaluating (7), we have to find the electric potential in the problem domain and the value of the viscous coefficient as a function of the orientation of the nanowire and

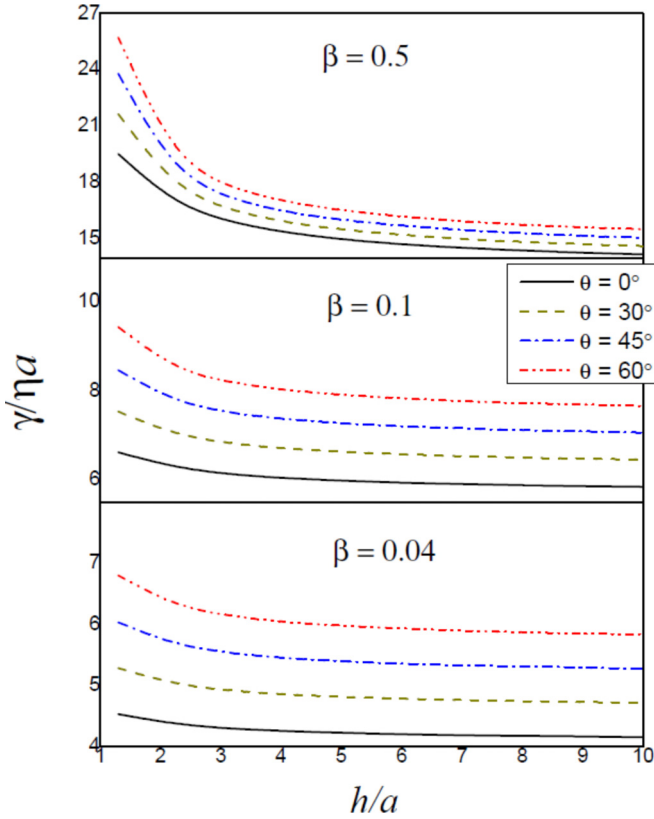


FIG. 3. Numerical results for $\gamma/\eta a$ as a function of the nondimensional distance to the bottom wall (h/a) for different orientations of the cylinder and aspect ratios $\beta = 0.04, 0.1, 0.5$. The cylinder aspect ratio is $\beta = b/a$.

the distance from the wall. We have used COMSOL MULTIPHYSICS to solve these two problems for cylinders with aspect ratios $\beta = \{0.04, 0.10, 0.50\}$. To this end, the equations are made nondimensional according to the following scales: a for distances, aE_0 for the electric potential, and $\varepsilon a E_0^2/\eta$ for velocities.

A. Viscous friction coefficient

For calculating the nondimensional viscous friction coefficient $\gamma/\eta a$, we have solved the nondimensional Stokes equations ($\nabla^2 \mathbf{v} - \nabla P = 0$; $\nabla \cdot \mathbf{v} = 0$) in the problem domain with boundary conditions of $\mathbf{v} = 1\mathbf{u}_x$ on the surface of the particle and $\mathbf{v} = 0$ on all other boundaries. In other words, we have found the flow field due to a cylinder moving with velocity $\mathbf{U} = 1\mathbf{u}_x$. From this solution, we have found the force on the particle by integrating the surface stress on the particle surface S , $\mathbf{F} = \int_S (\mathbf{n} \cdot \mathbb{T}) dS$. This force has, in general, nonzero vertical and horizontal components. We are only interested in the horizontal component, which corresponds to the denominator in Eq. (7).

Figure 3 shows the numerical results for $\gamma/\eta a$ as a function of the nondimensional distance to the bottom wall (h/a) for different orientations of the nanowire from parallel to the wall ($\theta = 0^\circ$) to perpendicular ($\theta = 90^\circ$). We show the results of $\gamma/\eta a$ for the three values of the aspect ratio that we will consider in the ICEP velocity. As expected, the viscous coefficient is highest when the particle is vertical and increases as the

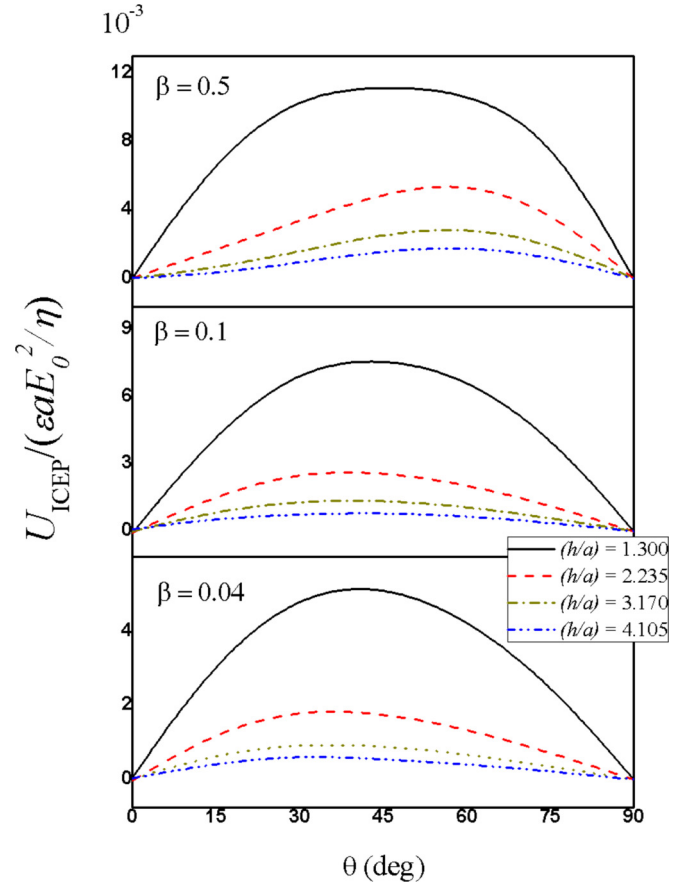


FIG. 4. U_{ICEP} as a function of the cylinder orientation for different heights over the insulating wall.

particle approaches the wall. Also, thicker rods have larger values of the nondimensional viscous coefficient. As a check of our numerical results, we have included Appendix A with a comparison with analytical approximations for the viscous coefficient of a cylinder in the liquid bulk.

B. Particle velocity as a function of its orientation

As described in the theory section, we use the reciprocity theorem [Eq. (7)] to calculate the ICEP velocity of the nanowire. First, the solution of the electric potential is used to evaluate the slip velocity on the surface of the cylinder [Eq. (6)]. Then, the solution of the Stokes equations mentioned above is used for evaluating the hydrodynamic stress tensor and calculating the numerator of Eq. (7). Figure 4 shows the results of U_{ICEP} as a function of the orientation of the nanowire for different positions on the insulating wall. As expected, the ICEP velocity is zero when the particle is either parallel or perpendicular to the insulating wall. Otherwise, the numerical results predict the movement of the nanowire so that its side closest to the wall leads, in accordance with the heuristic model above.

C. Particle velocity as a function of distance to the wall

In order to show the dependence of the particle velocity with its height, Fig. 5 shows the results of U_{ICEP} as a function

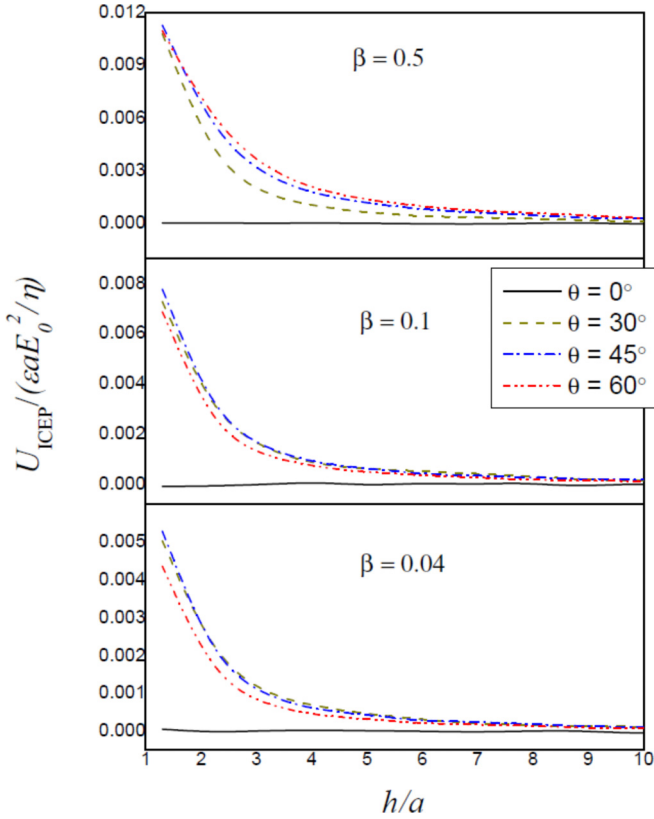


FIG. 5. U_{ICEP} as a function of the nondimensional distance to the bottom wall (h/a) for different orientations of the cylinder.

of the position over the insulating wall for different orientations. As expected, the ICEP velocity increases as the particle approaches the wall. Again, the ICEP velocity is zero when the particle is either parallel or perpendicular to the wall.

D. Fluid velocity field around the cylinder

The velocity field in the electrolyte can be found by solving the Stokes equations with boundary condition for the fluid velocity on the particle surface given by $\mathbf{v} = \mathbf{v}_s + \mathbf{U}_{\text{ICEP}}$, where \mathbf{v}_s is given by (6) and \mathbf{U}_{ICEP} is the ICEP velocity of the cylinder obtained in previous sections (IV B and IV C). Zero slip velocity ($\mathbf{v} = 0$) is imposed on all other boundaries.

Figure 6 shows the streamlines in a vertical plane that contains the cylinder axis. In this case, the aspect ratio of the cylinder is $\beta = 0.5$ and its height and orientation are, respectively, $(h/a) = 1.3$ and $\theta = 45^\circ$. The streamlines asymmetry due to the presence of the wall leads to a net horizontal motion of the particle.

V. DISCUSSION

We can compare the numerical results with the prediction of the heuristic model in Sec. II if we write the ICEP velocity of the composite particle [Eq. (1)] as a function of the height of the middle point of the composite particle, $h = h_1 + (d/2) \sin \theta = h_2 - (d/2) \sin \theta$:

$$\frac{U_{\text{ICEP}}}{\frac{d}{2} \varepsilon E_0^2 / 2\eta} = \frac{9}{32} \frac{2\beta \sin 2\theta}{(2h/d)^2 - (\sin \theta)^2}, \quad (8)$$

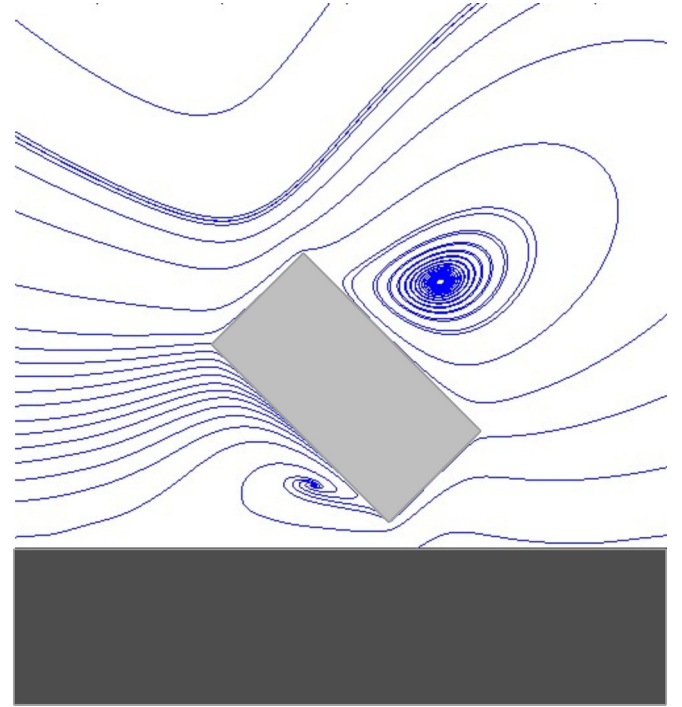


FIG. 6. Streamlines around a cylinder with aspect ratio $\beta = 0.5$. The height and orientation of the cylinder are, respectively, $(h/a) = 1.3$ and $\theta = 45^\circ$.

where we have defined the aspect ratio of the composite particle as $\beta = 2R/d$, in analogy with the case of the cylinder.

Figures 7 and 8 show the predictions of the heuristic model for U_{ICEP} as a function of, respectively, the height and orientation of the composite particle. For a closer comparison with the numerical results, we show in Figs. 9 and 10 the predictions of the heuristic model for two different heights and the numerical results for two cylinders with aspect ratios $\beta = 0.04$ (as in experiments of Ref. [40]) and $\beta = 0.5$, which corresponds to a thick cylinder. Note that β has been included in the scale of the ICEP velocity. This comparison confirms that the heuristic model is not only useful for predicting the qualitative behavior of the metal rods, it also provides a very good approximation to U_{ICEP} for metal rods close to the bottom wall.

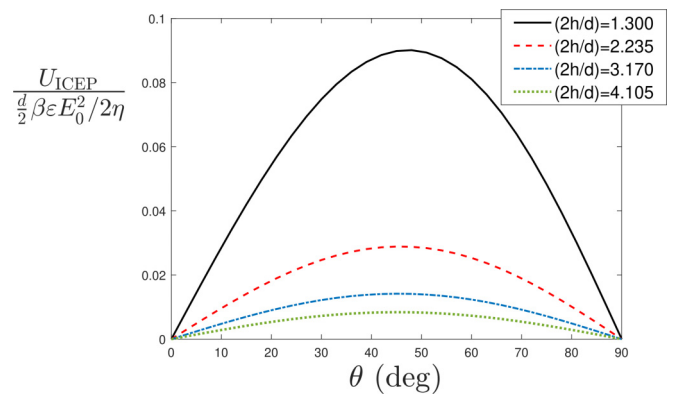


FIG. 7. U_{ICEP} as a function of orientations for the heuristic model.

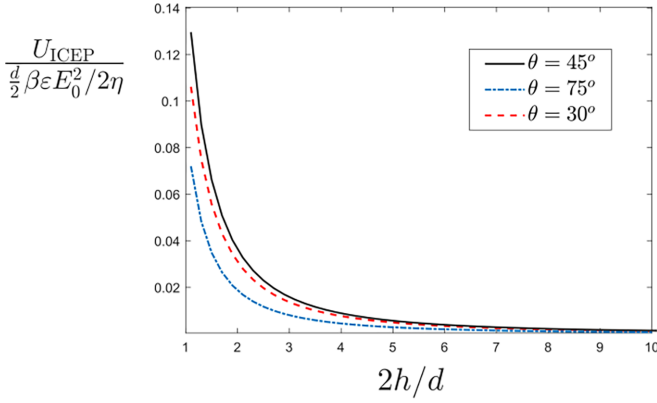


FIG. 8. U_{ICEP} as a function of height for the heuristic model.

It is also interesting to estimate a dimensional value of U_{ICEP} for typical experimental conditions. For a nanowire with $\beta = 0.04$ as in Ref. [40], the maximum velocity is obtained when $\theta \approx 45^\circ$. We observe in Fig. 4 that $[U_{ICEP}/(\epsilon a E_0^2/\eta)] \approx 5.0 \times 10^{-3}$, for $h/a = 1.3$ and $\theta \approx 45^\circ$. Considering that the typical maximum value for the amplitude of the electric field in electrokinetic experiments is $E_0 \approx 100$ kV/m and considering that $a = 3.5$ μm for nanowires in [40], the maximum value for the ICEP velocity is $U_{ICEP} \approx 120$ $\mu\text{m/s}$. However, it is well known that the ICEO velocity on real metal-electrolyte interfaces is lower than the value predicted by Eq. (6), sometimes by one order of magnitude [49]. Several possible causes have been proposed in the literature for the reduction of slip velocity: a dielectric oxide layer on the metal [50,51], ion adsorption [50,52], counterion crowding [49], surface roughness [53], surface conduction [54], and/or residual Faradaic reactions [55,56]. All these phenomena can lead to a reduction of the effective ζ potential and therefore it is more reasonable to expect maximum velocities on the order of tens of micron/s in experiments.

VI. CONCLUSIONS

We have shown theoretically that a metal microscopic cylinder immersed in an electrolyte and subjected to an electric field translates parallel to an insulating wall. The origin

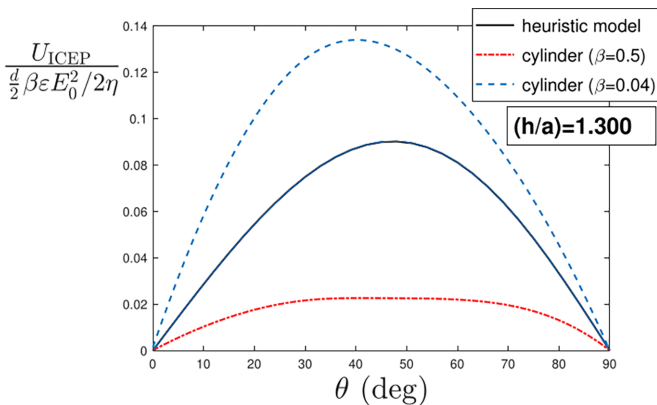


FIG. 9. U_{ICEP} as a function of orientation for the heuristic model and for two cylinders with aspect ratios $\beta = 0.04$ and $\beta = 0.5$, $h/a = 1.300$.

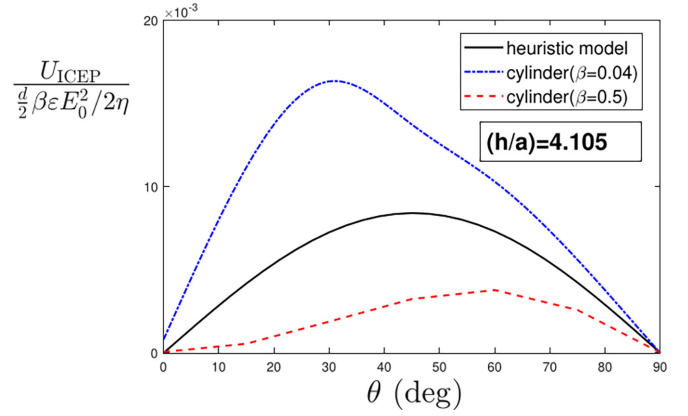


FIG. 10. U_{ICEP} as a function of orientation for the heuristic model and for two cylinders with aspect ratios $\beta = 0.04$ and $\beta = 0.5$, $h/a = 4.105$.

of this motion is the wall-particle interaction that arises from the ICEO on the cylinder surface. The applied electric field could be dc or low-frequency ac and a net motion of the particle is expected as long as the cylinder axis is inclined with respect to the wall. To develop a physical intuition of the phenomenon, we have included analytical results for a heuristic model consisting of two metal spheres connected by a thin metal wire. The predictions of this model are in qualitative agreement with numerical simulations of a metal cylinder. The model predicts that the cylinder side closest to the wall leads the particle motion. Also, the heuristic model is used for obtaining quantitative predictions of the particle velocity, which are close to the exact numerical solutions.

We have shown numerical results of the velocity of the cylinder as a function of its orientation and distance from the wall. In general, the velocity decreases with distance and its maximum value is found for an orientation that depends on the particle aspect ratio, β . For example, for a nanowire with $\beta = 0.04$, the maximum particle velocity is found for an inclination of $\approx 45^\circ$. For such slender nanowires with lengths around 6 or 7 micron, we have estimated that particle velocities of tens of microns per second can be expected in realistic conditions, i.e., considering the reduction of ICEO velocities in real metal-electrolyte interfaces. Even larger velocities are expected for thicker nanowires if the particle orientation is controlled.

ACKNOWLEDGMENTS

A.R. and P.G.S. acknowledge financial support by MCIN/AEI/10.13039/501100011033/FEDER, UE (Grant No. PID2022-138890NB-I00). J.E.F.M. acknowledges financial support from 100017966-VIEP-BUAP-2022 under Contract No. FLMJ-ING22-G.

APPENDIX A: VISCOUS FRICTION COEFFICIENTS OF A CYLINDER IN THE LIQUID BULK: COMPARISON BETWEEN NUMERICAL AND ANALYTICAL RESULTS

In this section, we compare our numerical results for the nondimensional viscous coefficient ($\gamma/\eta a$) of cylinders far

TABLE I. Comparison between numerical values for the viscous friction coefficients and the predictions of analytical approximations found in the literature for cylinders with $\beta = 0.04, 0.1, 0.5$.

Cylinder aspect ratio	$\beta = 0.04$		$\beta = 0.1$		$\beta = 0.5$	
	$\gamma_{\parallel}/\eta a$	$\gamma_{\perp}/\eta a$	$\gamma_{\parallel}/\eta a$	$\gamma_{\perp}/\eta a$	$\gamma_{\parallel}/\eta a$	$\gamma_{\perp}/\eta a$
Numerical results	4.12427	6.32339	5.79246	8.15949	13.86325	15.5594
Tirado <i>et al.</i> [57]	4.11896	6.18173	5.73217	7.94733	13.3274	14.9342
Broersma [58]	4.6396	6.64978	7.2332	9.0610	9.1222	16.156

from the wall with the predictions of analytical approximations. Tirado *et al.* [57] report the following expressions for the viscous coefficient of a slender cylinder moving in either the direction of its symmetry axis (γ_{\parallel}) or perpendicular to it (γ_{\perp}):

$$\gamma_{\parallel} = \frac{4\pi\eta a}{\ln(1/\beta + \nu_{\parallel})}, \quad \gamma_{\perp} = \frac{8\pi\eta a}{\ln(1/\beta + \nu_{\perp})}, \quad (\text{A1})$$

with $\nu_{\parallel} = -0.207 + 0.980\beta - 0.133\beta^2$ and $\nu_{\perp} = 0.839 + 0.185\beta + 0.233\beta^2$.

Before the work of Tirado *et al.*, Broersma [58,59] reported the same equations (A1) but with different expressions for the coefficients ν_{\parallel} and ν_{\perp} . The coefficients reported in Ref. [58] are $\nu_{\parallel}(\text{Broersma}) = -0.114 - 0.15/\ln(2/\beta) - 13.5/\ln^2(2/\beta) + 37/\ln^3(2/\beta) - 22/\ln^4(2/\beta)$ and $\nu_{\perp}(\text{Broersma}) = 0.886 - 0.15/\ln(2/\beta) - 8.1/\ln^2(2/\beta) + 18/\ln^3(2/\beta) - 9/\ln^4(2/\beta)$.

Table I shows a comparison between our exact numerical results for $\gamma/\eta a$ and the predictions of the two analytical approximations. The agreement between the approximation of Tirado *et al.* and the numerical results is excellent for slender cylinders ($\beta = 0.04$) and it remains very good for cylinders as thick as $\beta = 0.5$.

APPENDIX B: DYNAMICS OF A FREELY ROTATING AND TRANSLATING CYLINDER

In this Appendix, we describe how to tackle the study of the dynamics of a cylinder immersed in a viscous liquid. The fluid velocity on the cylinder surface can be written as $\mathbf{v} = \mathbf{v}_s + \mathbf{U} + \boldsymbol{\Omega} \times \mathbf{r}$, where \mathbf{U} is the translational velocity of the center of mass, $\boldsymbol{\Omega}$ is the angular velocity, and \mathbf{r} is the position vector from the center of mass. For simplicity, we restrict the motion of the cylinder center to the xz plane of Fig. 2, that is, $\mathbf{U} = U_x \mathbf{u}_x + U_z \mathbf{u}_z$, $\boldsymbol{\Omega} = \Omega \mathbf{u}_y$. Let us consider the following velocity fields: the flow induced by the slip velocity on a stationary cylinder near the wall (problem 1) and the flow generated by the translating and rotating cylinder with zero slip velocity at the same position and orientation (problem 2). The cylinder velocity is \mathbf{V} and its angular velocity is $\boldsymbol{\Sigma}$. The Lorentz reciprocal theorem reads [46,60]

$$\int_S \mathbf{n} \cdot [\mathbb{T}_1 \cdot (\mathbf{V} + \boldsymbol{\Sigma} \times \mathbf{r})] dS = \int_S \mathbf{n} \cdot (\mathbb{T}_2 \cdot \mathbf{v}_s) dS, \quad (\text{B1})$$

where \mathbb{T}_1 and \mathbb{T}_2 are, respectively, the hydrodynamic stress tensors that arise from the flow fields of problem 1 and problem 2. The integrals are carried out only on the particle surface since the velocity is zero at the plane wall. Let problem 2 be

the one generated by $\mathbf{V} = 1\mathbf{u}_x$ and $\boldsymbol{\Sigma} = 0$. Thus we have

$$\int_S \mathbf{n} \cdot (\mathbb{T}_1 \cdot \mathbf{u}_x) dS = \int_S \mathbf{n} \cdot (\mathbb{T}_X \cdot \mathbf{v}_s) dS, \quad (\text{B2})$$

where $\mathbb{T}_2 = \mathbb{T}_X$, the hydrodynamic stress tensor corresponding to the cylinder moving along the x direction. In the same manner, we define \mathbb{T}_Z and \mathbb{T}_{Ω} , respectively, as the hydrodynamic stress tensors for problem 2 with translation along z ($\mathbf{V} = 1\mathbf{u}_z$, $\boldsymbol{\Sigma} = 0$) and rotation around y ($\mathbf{V} = 0$, $\boldsymbol{\Sigma} = 1\mathbf{u}_y$). On the left-hand side of Eq. (B2), we can recognize the x component of hydrodynamic force on the cylinder generated by the slip velocity. The balance of forces along the x direction together with the linearity of Stokes solutions allows us to write

$$F_x = \int_S \mathbf{n} \cdot (\mathbb{T}_1 \cdot \mathbf{u}_x) dS + U_x \int_S \mathbf{n} \cdot (\mathbb{T}_X \cdot \mathbf{u}_x) dS + U_z \int_S \mathbf{n} \cdot (\mathbb{T}_Z \cdot \mathbf{u}_x) dS + \Omega \int_S \mathbf{n} \cdot (\mathbb{T}_{\Omega} \cdot \mathbf{u}_x) dS, \quad (\text{B3})$$

where F_x is the x component of the external force. On the right-hand side, we can recognize the x component of hydrodynamic force on the cylinder with $\mathbf{v} = \mathbf{v}_s + \mathbf{U} + \boldsymbol{\Omega} \times \mathbf{r}$ on its surface. Inserting this into Eq. (B2), we arrive at

$$F_x - \int_S \mathbf{n} \cdot (\mathbb{T}_X \cdot \mathbf{v}_s) dS = U_x \int_S \mathbf{n} \cdot (\mathbb{T}_X \cdot \mathbf{u}_x) dS + U_z \int_S \mathbf{n} \cdot (\mathbb{T}_Z \cdot \mathbf{u}_x) dS + \Omega \int_S \mathbf{n} \cdot (\mathbb{T}_{\Omega} \cdot \mathbf{u}_x) dS. \quad (\text{B4})$$

The process is repeated for problem 2 with $\mathbf{V} = 1\mathbf{u}_z$, $\boldsymbol{\Sigma} = 0$, and we obtain

$$F_z - \int_S \mathbf{n} \cdot (\mathbb{T}_Z \cdot \mathbf{v}_s) dS = U_x \int_S \mathbf{n} \cdot (\mathbb{T}_X \cdot \mathbf{u}_z) dS + U_z \int_S \mathbf{n} \cdot (\mathbb{T}_Z \cdot \mathbf{u}_z) dS + \Omega \int_S \mathbf{n} \cdot (\mathbb{T}_{\Omega} \cdot \mathbf{u}_z) dS. \quad (\text{B5})$$

Finally, taking as problem 2 a rotation around y ($\mathbf{V} = 0$, $\boldsymbol{\Sigma} = 1\mathbf{u}_y$) and equilibrium of torques, we arrive at

$$N - \int_S \mathbf{n} \cdot (\mathbb{T}_{\Omega} \cdot \mathbf{v}_s) dS = U_x \mathbf{u}_y \cdot \int_S \mathbf{r} \times (\mathbb{T}_X \cdot \mathbf{n}) dS + U_z \mathbf{u}_y \cdot \int_S \mathbf{r} \times (\mathbb{T}_Z \cdot \mathbf{n}) dS + \Omega \mathbf{u}_y \cdot \int_S \mathbf{r} \times (\mathbb{T}_{\Omega} \cdot \mathbf{n}) dS, \quad (\text{B6})$$

where N is the external torque along the y direction.

The system of equations (B4)–(B6) allows us to obtain the cylinder velocities (U_x, U_y, Ω) . In our case of a cylinder subjected to an electric field, (F_x, F_y, N) are the components of the electrical force and torque applied to the particle and we computed them using integration of the Maxwell stress tensor.

As an example we have obtained (U_x, U_y, Ω) for the case of a nanowire with the following parameters: $\beta = 0.1$, $\theta = 45^\circ$, and $h/a = 2$. The velocities are $(U_x, U_y) = (0.00307, -0.00163)\varepsilon a E_0^2/\eta$, $\Omega = -0.224 \varepsilon E_0^2/\eta$ and these values are almost coincident with those without considering the external electrical force and torque. In this case of $\beta = 0.1$, the cylinder is slender and the electric field lines are only slightly perturbed and, hence, the electric field generates negligible stresses [19,23]. In other words, the motion is mainly due to ICEP. The nondimensional angular velocity is much greater than the nondimensional translational velocity. This means that the nanowire aligns with the electric field much faster than it moves. In addition, the

faster rotation gives rise to a negative velocity along the z direction, i.e., the cylinder center of mass approaches the wall.

In this situation, if the nanowire is not allowed to rotate $(U_x, U_y) = (0.00342, 0.00417)\varepsilon a E_0^2/\eta$, it turns out that there is hydrodynamic repulsion from the wall as well as horizontal motion. Also, if the nanowire can only move along the x direction as in the main text of this paper, $U_x = 0.00429\varepsilon a E_0^2/\eta$.

We consider another example for the same nanowire but closer to the wall ($\beta = 0.1$, $\theta = 45^\circ$, and $h/a = 1$). The result in this case is $(U_x, U_y, a\Omega) = (0.0142, -0.0137, -0.218)\varepsilon a E_0^2/\eta$. Again, the nanowire is aligned with the electric field much faster than it moves. If the nanowire is not allowed to rotate $(U_x, U_y) = (0.0190, 0.0107)\varepsilon a E_0^2/\eta$. Finally, if the nanowire can only move along the x direction $U_x = 0.0217\varepsilon a E_0^2/\eta$. The velocities of translation are higher because the nanowire is closer to the wall, while the angular velocity is slightly lower.

-
- [1] R. Hunter, *Introduction to Modern Colloid Science* (Oxford University Press, Oxford, 1993).
- [2] M. von Smoluchowski, *Bull. Akad. Sci. Cracovie.* **8**, 182 (1903).
- [3] R. W. O'Brien and L. R. White, *J. Chem. Soc. Faraday Trans. 2* **74**, 1607 (1978).
- [4] E. M. Southern, *J. Mol. Biol.* **98**, 503 (1975).
- [5] S. Gangwal, O. J. Cayre, M. Z. Bazant, and O. D. Velev, *Phys. Rev. Lett.* **100**, 058302 (2008).
- [6] M. Z. Bazant and T. M. Squires, *Phys. Rev. Lett.* **92**, 066101 (2004).
- [7] J. A. Levitan, S. Devasenathipathy, V. Studer, Y. Ben, T. Thorsen, T. M. Squires, and M. Z. Bazant, *Colloids Surf. A* **267**, 122 (2005).
- [8] T. Squires and M. Bazant, *J. Fluid Mech.* **560**, 65 (2006).
- [9] A. M. Boymelgreen and T. Miloh, *Phys. Fluids* **23**, 072007 (2011).
- [10] A. Boymelgreen, G. Yossifon, S. Park, and T. Miloh, *Phys. Rev. E* **89**, 011003(R) (2014).
- [11] A. M. Boymelgreen, T. Balli, T. Miloh, and G. Yossifon, *Nat. Commun.* **9**, 760 (2018).
- [12] F. Katzmeier and F. C. Simmel, *Nat. Commun.* **14**, 6247 (2023).
- [13] V. Calero, R. Fernández-Mateo, H. Morgan, P. García-Sánchez, and A. Ramos, *Phys. Rev. Appl.* **15**, 014047 (2021).
- [14] R. Fernández-Mateo, P. García-Sánchez, V. Calero, H. Morgan, and A. Ramos, *J. Fluid Mech.* **924**, R2 (2021).
- [15] A. Boymelgreen, G. Yossifon, and T. Miloh, *Langmuir* **32**, 9540 (2016).
- [16] A. M. Boymelgreen, G. Kunti, P. García-Sánchez, A. Ramos, G. Yossifon, and T. Miloh, *J. Colloid Interface Sci.* **616**, 465 (2022).
- [17] M. S. Kilic and M. Z. Bazant, *Electrophoresis* **32**, 614 (2011).
- [18] F. Ma, X. Yang, H. Zhao, and N. Wu, *Phys. Rev. Lett.* **115**, 208302 (2015).
- [19] J. J. Arcenegui, P. García-Sánchez, H. Morgan, and A. Ramos, *Phys. Rev. E* **88**, 063018 (2013).
- [20] J. J. Arcenegui, P. García-Sánchez, H. Morgan, and A. Ramos, *Phys. Rev. E* **89**, 062306 (2014).
- [21] M. A. Haque, X. Zhu, N. Uyanga, and N. Wu, *Langmuir* **39**, 2751 (2023).
- [22] P. García-Sánchez and A. Ramos, *Langmuir* **33**, 8553 (2017).
- [23] J. E. Flores-Mena, P. García-Sánchez, and A. Ramos, *Phys. Rev. E* **99**, 032603 (2019).
- [24] P. García-Sánchez, J. J. Arcenegui, H. Morgan, and A. Ramos, *Appl. Phys. Lett.* **106**, 023110 (2015).
- [25] D. Saintillan, E. Darvel, and E. Shaqfeh, *J. Fluid Mech.* **563**, 223 (2006).
- [26] K. A. Rose, J. A. Meier, G. M. Dougherty, and J. G. Santiago, *Phys. Rev. E* **75**, 011503 (2007).
- [27] P. A. Smith, C. D. Nordquist, T. N. Jackson, T. S. Mayer, B. R. Martin, J. Mbindyo, and T. E. Mallouk, *Appl. Phys. Lett.* **77**, 1399 (2000).
- [28] R. Krupke, F. Hennrich, H. v. Löhneysen, and M. M. Kappes, *Science* **301**, 344 (2003).
- [29] C. Akin, L. C. Feldman, C. Durand, S. M. Hus, A.-P. Li, H. Y. Hui, M. A. Filler, J. Yi, and J. W. Shan, *Lab Chip* **16**, 2126 (2016).
- [30] C. Akin, J. Yi, L. C. Feldman, C. Durand, S. M. Hus, A.-P. Li, M. A. Filler, and J. W. Shan, *ACS Nano* **9**, 5405 (2015).
- [31] J. Boote and S. Evans, *Nanotechnology* **16**, 1500 (2005).
- [32] B. Edwards, T. S. Mayer, and R. B. Bhiladvala, *Nano Lett.* **6**, 626 (2006).
- [33] A. Ramos, P. García-Sánchez, and H. Morgan, *Curr. Opin. Colloid Interface Sci.* **24**, 79 (2016).
- [34] J. J. Arcenegui, P. García-Sánchez, H. Morgan, and A. Ramos, *Electrophoresis* **34**, 979 (2013).
- [35] P. García-Sánchez, Y. Ren, J. J. Arcenegui, H. Morgan, and A. Ramos, *Langmuir* **28**, 13861 (2012).
- [36] L. Rodríguez-Sánchez, A. Ramos, and P. García-Sánchez, *Phys. Rev. E* **100**, 042616 (2019).
- [37] H.-J. Keh and J. Anderson, *J. Fluid Mech.* **153**, 417 (1985).
- [38] J. Happel and H. Brenner, *Low Reynolds Number Hydrodynamics: With Special Applications to Particulate Media* (Springer Science & Business Media, New York, 2012), Vol. 1.
- [39] V. G. Levich, *Physicochemical Hydrodynamics* (Prentice-Hall, Englewood Cliffs, NJ, 1962).

- [40] J. J. Arcenegui, P. García-Sánchez, H. Morgan, and A. Ramos, *Phys. Rev. E* **88**, 033025 (2013).
- [41] A. Ramos, H. Morgan, N. Green, and A. Castellanos, *J. Colloid Interface Sci.* **217**, 420 (1999).
- [42] A. González, A. Ramos, N. G. Green, A. Castellanos, and H. Morgan, *Phys. Rev. E* **61**, 4019 (2000).
- [43] T. Miloh, *Phys. Fluids* **20**, 107105 (2008).
- [44] M. Teubner, *J. Chem. Phys.* **76**, 5564 (1982).
- [45] M. Fair and J. Anderson, *J. Colloid Interface Sci.* **127**, 388 (1989).
- [46] H. A. Stone and A. D. T. Samuel, *Phys. Rev. Lett.* **77**, 4102 (1996).
- [47] J. E. Flores-Mena, P. García-Sánchez, and A. Ramos, *Micromachines* **11**, 259 (2020).
- [48] P. García-Sánchez and A. Ramos, *Phys. Rev. E* **92**, 052313 (2015).
- [49] M. Z. Bazant, M. S. Kilic, B. D. Storey, and A. Ajdari, *Adv. Colloid Interface Sci.* **152**, 48 (2009).
- [50] A. J. Pascall and T. M. Squires, *Phys. Rev. Lett.* **104**, 088301 (2010).
- [51] N. G. Green, A. Ramos, A. González, H. Morgan, and A. Castellanos, *Phys. Rev. E* **66**, 026305 (2002).
- [52] Y. K. Suh and S. Kang, *Phys. Rev. E* **79**, 046309 (2009).
- [53] R. J. Messinger and T. M. Squires, *Phys. Rev. Lett.* **105**, 144503 (2010).
- [54] O. Schnitzer and E. Yariv, *Phys. Rev. E* **86**, 021503 (2012).
- [55] L. H. Olesen, H. Bruus, and A. Ajdari, *Phys. Rev. E* **73**, 056313 (2006).
- [56] A. Ramos, A. González, P. García-Sánchez, and A. Castellanos, *J. Colloid Interface Sci.* **309**, 323 (2007).
- [57] M. M. Tirado, C. L. Martínez, and J. G. de la Torre, *J. Chem. Phys.* **81**, 2047 (1984).
- [58] S. Broersma, *J. Chem. Phys.* **74**, 6989 (1981).
- [59] S. Broersma, *J. Chem. Phys.* **32**, 1632 (1960).
- [60] H. Masoud and H. A. Stone, *J. Fluid Mech.* **741**, R4 (2014).